Supplementary Information (SI) for Journal of Materials Chemistry A.
This journal is © The Royal Society of Chemistry 2026

Supporting Information

Proton-conducting hydrogen-bonded nanochannels encapsulating perylene-based photocatalysts for solar hydrogen evolution

Hua Chai[2,4], Yan Guo[3], Jun Nan[4], Yongfa Zhu[2], Qixin Zhou[1,2 *]

1 Department of Materials Science and Engineering, City University of Hong Kong, Hong Kong, China

E-mail: Qixin.Zhou@cityu.edu.hk

2 Department of Chemistry, Tsinghua University

3 Department of Civil Engineering, The University of Hong Kong, Hong Kong, China

4 State Key Laboratory of Urban Water Resource and Environment, School of Environment, Harbin Institute of Technology, Harbin, China

Table of Contents

1. Experimental Procedures

1.1 Materials

3,4,9,10-Perylenetetracarboxylic dianhydride (PTCDA), chloroplatinic(IV) acid (H_2PtCl_6), ascorbic acid (AA), N, N-dimethylformamide (DMF), and acetone were purchased from Alfa Aesar. All the reagents used for photocatalytic syntheses were of reagent grade without further purification. Solvents for self-assembly were of high-performance liquid chromatography grade. Deionized water (DI) was used throughout the experiments.

1.2 Synthesis

Synthesis of HOF: The hydrogen-bonded organic framework (HOF) based on 1,3,6,8-tetrakis(p-benzoic acid)pyrene (H_4TBAPy) was synthesized following our previously reported method[1]. Briefly, 100 mg of H_4TBAPy solid was dissolved in 15 mL DMF under ultrasonic conditions. A mixture of 120 mL deionized water/ethanol (v/v = 1:1) was injected within 2 minutes, and the resulting solution was stirred at 1000 r/min for 6 h. The solid powder was washed repeatedly with deionized water and acetone, and then soaked in acetone at room temperature for 72 h to remove residual solvents from the micropores. Finally, the product was filtered and dried under vacuum at 60 °C for 8 h, yielding a bright yellow powder as the HOF.

Synthesis of PTCDA: PTCDA aggregates were prepared following our previously reported protocol[2]. Typically, 50 mg of commercial PTCDA was dispersed in 5 mL of sulfuric acid and sonicated for 1 h. Subsequently, 50 mL of deionized water was added, upon which a bright red solid immediately precipitated. The precipitate was collected by filtration, washed with deionized water until the filtrate reached neutrality, and then dried under vacuum at 60 °C. The solids were identified as the PTCDA.

Synthesis of PTCDA-in-HOF: 25 mg of highly crystalline PTCDA was uniformly dispersed in 100 mL of a deionized water/ethanol mixed solvent (volume ratio = 1:1) through ultrasonication to form a homogeneous suspension (denoted as solution A). Separately, 25 mg of H_4TBAPy was completely dissolved in 20 mL of DMF under magnetic stirring at room temperature, resulting in a clear solution B. Subsequently, solution B was slowly added dropwise to solution A under continuous stirring, allowing H_4TBAPy to undergo self-assembly and crystallize with PTCDA serving as the heterogeneous nucleation site. The resulting solid powder was washed repeatedly with deionized water and acetone, followed by soaking in acetone at room temperature for 72 h to remove residual solvents from the micropores. Finally, the

product was filtered and dried under vacuum at 60 °C, yielding an orange-red powder identified as PTCDA-in-HOF.

Synthesis of Pt-PTCDA-in-HOF: 100 mg of PTCDA-in-HOF was dispersed in 100 mL of water (5 °C), and 10 mL of H_2PtCl_6 (0.1 wt.%) was added and stirred vigorously. Subsequently, the above suspension was irradiated with full spectrum (≥ 350 nm, 100 mW cm^{-2}) for 1 h. Subsequently, the solid was isolated by filtration and washed with deionized water until the filtrate was neutral. The solid was collected and dried under vacuum at 60°C, which was Pt-PTCDA-in-HOF. The Pt content was determined to be 7.0 wt.% by ICP-MS (8800, Agilent Technologies). The same method was used to prepare Pt-PTCDA and Pt-HOF, respectively.

1.3 Characterization

The morphologies of the samples were investigated using cryo-TEM (G4i, cryo-TEM), transmission electron microscope (TEM, Hitachi HT7700), field emission scanning electron microscopy (FE-SEM, Hitachi SU-8010), and an atomic force microscope (AFM, Oxford Cypher VRS) with a high-resolution probe in Kelvin probe force microscopy (KPFM) mode. Powder X-ray diffraction (PXRD) patterns of the samples were obtained on a Bruker D8 Advance X-ray diffractometer using Cu Kα1 (λ = 1.54 Å) radiation at 45 kV and 200 mA. Fourier transform infrared spectra (FT-IR) with attenuated total reflection (ATR) were recorded on a Bruker V70 spectrometer. The surface areas were calculated by the Brunauer-Emmet-Teller (BET) instrument (MicroActive, ASAP 2460). Ultraviolet-visible (UV-vis) diffuse reflectance spectroscopy (DRS) spectra were acquired on a Hitachi U-3010 spectrophotometer with a reference of $BaSO_4$. The photoluminescence (PL) spectra were measured on an Edinburgh FS5 fluorescence spectrometer with an excitation wavelength of 360 nm. The catalytic products in the liquid phase were analysed using high-performance liquid chromatography-time-of-flight mass spectrometry (LCMS-TOF, Shimadzu).

Notably, all cryo-EM experiments were conducted using a Thermo Fisher Scientific Titan Krios G3i electron microscope operating at an accelerating voltage of 300 kV. The aqueous suspension of PTCDA-in-HOF was applied to microgrids and thoroughly vacuum-dried. The samples were then maintained in a liquid nitrogen environment and transferred to the cryo-EM using a cryotransfer loader. Cryo-EM images were acquired in counting mode with a K3 Summit Direct Electron Detector equipped with a GIF Quantum energy filter. To minimize structural damage to the hydrogen-bonded organic framework caused by the electron beam, the dose rate on the detector was set to approximately 15 counts per pixel per second, and the frame exposure time was approximately 23 ms. Each image represents a superposition of 10

automatically collected frames after motion correction, with a total dose of approximately 30 e^{-} $Å^{-2}$.

1.4 Experimental Methods

Surface photogenerated voltage (SPV) measurement mechanism.

The charge separation and migration ability of the photocatalyst were tested using the SPV device developed in the laboratory[3]. The instrument mainly consists of a phase-locked amplifier (SR830-DSP), a light chopper (SR540), a xenon light source (CHF-XQ500W), and a double prism monochromator (Omni-λ3005). The width of the slit is set to 3 mm. The structure of the photovoltage sample cell is ITO glass - sample - ITO glass.

Photoelectrochemical measurements

5 mg of the photocatalyst was dispersed in a mixed solution containing 1 mL of ethanol and 10 μL of Nafion solution, followed by ultrasonic treatment for 30 min to form a homogeneous ink. To prepare the working electrode, the as-prepared ink was uniformly coated onto an indium tin oxide (ITO) glass substrate, with the effective working area controlled at 1×1 cm^2. The coated substrate was then dried at 60 °C to obtain the final working electrode. Photoelectrochemical measurements were conducted on an electrochemical workstation (CHI660E, Chenhua Instrument Co., Ltd., Shanghai, China) using a standard three-electrode system. In this system, the prepared ITO-based electrode served as the working electrode, a platinum wire as the counter electrode, and an Ag/AgCl electrode as the reference electrode. The electrolyte used was a 0.1 mol L^{-1} Na_2SO_4 aqueous solution.

Photocatalytic H_2 evolution

The photocatalytic H_2 evolution was performed in a Pyrex top-irradiation reaction vessel with a stationary temperature of 25 °C. The reaction vessel was connected to a glass closed gas system (Labsolar-6A, Beijing Perfectlight). Typically, 2.5 mg photocatalyst was added to a 100 ml aqueous solution containing 3.52 g AA and 7 wt% Pt as a co-catalyst was loaded onto the photocatalyst by the in situ photo-deposition method using H_2PtCl_6. A 300 W Xe lamp was used as the light source, and the irradiation intensity was ~500 mW cm^{-2}. The evolved H_2 was determined using a gas chromatograph (GC7920, TCD, Ar carrier).

2. Additional Supplementary Figures

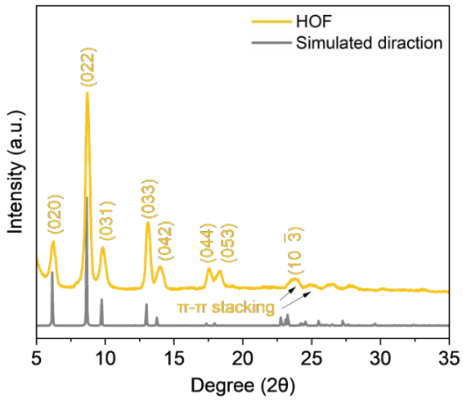

Fig. S1 PXRD pattern and simulated diffraction pattern of HOF.

The PXRD pattern (**Fig. S1**) of the as-prepared HOF closely matches its simulated diffraction pattern in both peak positions and relative intensities, providing clear evidence of the high phase purity of the synthesized HOF sample.

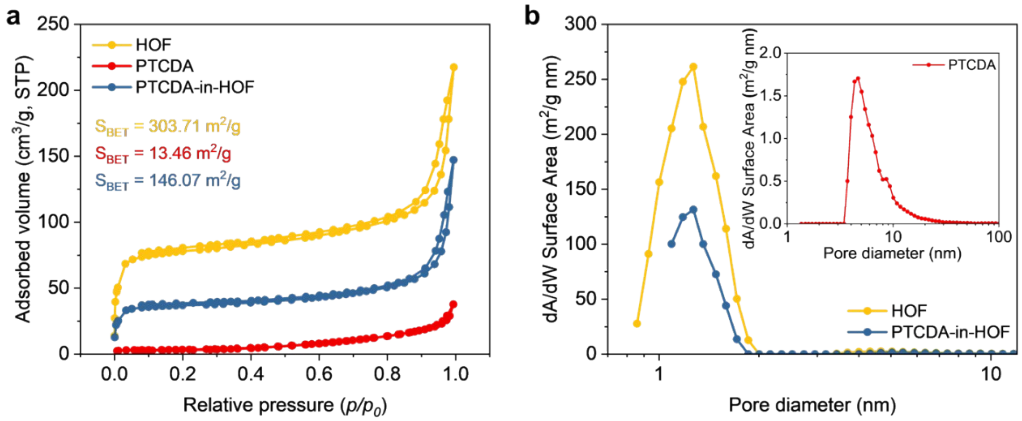

Fig. S2 (a) N_2 adsorption-desorption isotherms and (b) pore size distribution of HOF, PTCDA, and PTCDA-in-HOF. The relevant detailed information is summarized in **Table S1**.

The porosity of HOF, PTCDA, and PTCDA-in-HOF was evaluated using N_2 sorption measurements at 77.3 K. The Brunauer–Emmett–Teller (BET) surface areas were determined to be 303.71 $m^2\ g^{-1}$, 13.46 $m^2\ g^{-1}$, and 146.07 $m^2\ g^{-1}$, respectively (**Fig. S2a**). Compared to the organic semiconductor PTCDA, HOF exhibits excellent porosity. However, when coated with PTCDA, some of the voids in HOF are blocked, resulting in a significant reduction in its BET surface area. The mean pore sizes of HOF, PTCDA, and PTCDA-in-HOF, obtained by fitting the N_2 isotherms with N_2-DFT models, were 1.26 nm, 4.72 nm, and 1.32 nm, respectively (**Fig. S2b**).

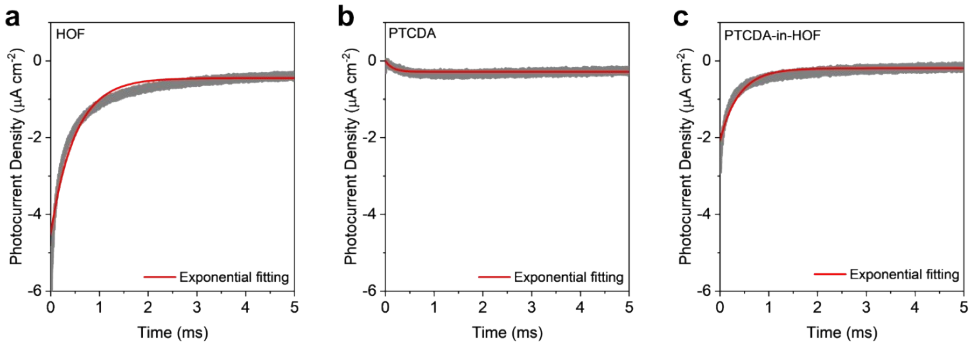

Fig. S3 Transient photocurrent spectra and exponential fitting curve of (a) HOF, (b) PTCDA, and (c) PTCDA-in-HOF.

The current decay curve was fitted using a single exponential function, equation (1):

$$I(t) = I(0) \times e^{-t/\tau} \quad (1)$$

where I(t) denotes the transient photocurrent at time t (μA cm^{-2}), I(0) represents the initial photocurrent at t = 0 (μA cm^{-2}), and τ stands for the current decay time constant (ms). Based on the exponential fitting of transient photocurrent decay curves, the decay times of HOF, PTCDA, and PTCDA-in-HOF were determined to be 0.50 ms, 0.15 ms, and 0.39 ms, respectively (**Fig. S3**).

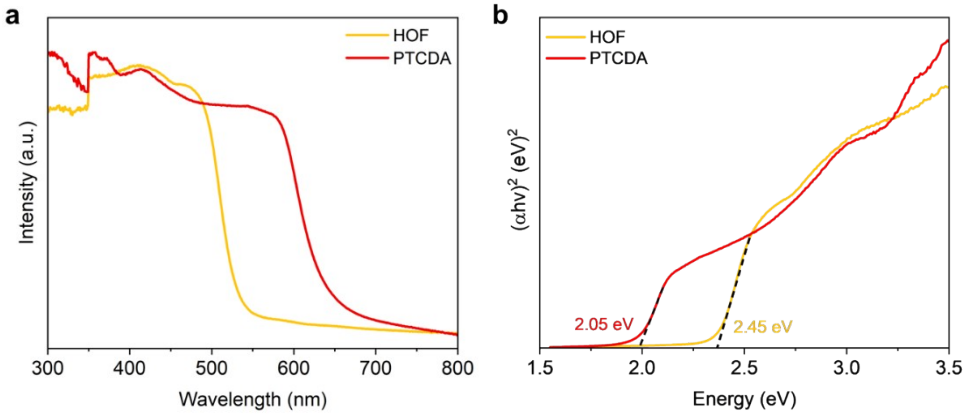

Fig. S4 (a) UV-Vis absorption spectrum and (b) corresponding Tauc plots of HOF and PTCDA.

UV-Vis DRS was employed to assess the light-harvesting performance of HOF and PTCDA. As shown in **Fig. S4a**, the absorption edge of HOF is approximately 540 nm, whereas that of PTCDA is red-shifted to around 650 nm, indicating that PTCDA exhibits superior absorption in the visible light region. Using the Tauc plot (**Fig. S4b**), the optical band gaps of HOF and PTCDA were determined to be 2.45 eV and 2.05 eV, respectively. PTCDA not only possesses a broader spectral response range but also a smaller band gap energy, enabling it to function as an efficient light-harvesting unit in composite materials and significantly expanding the solar spectrum utilization range of the PTCDA-in-HOF system.

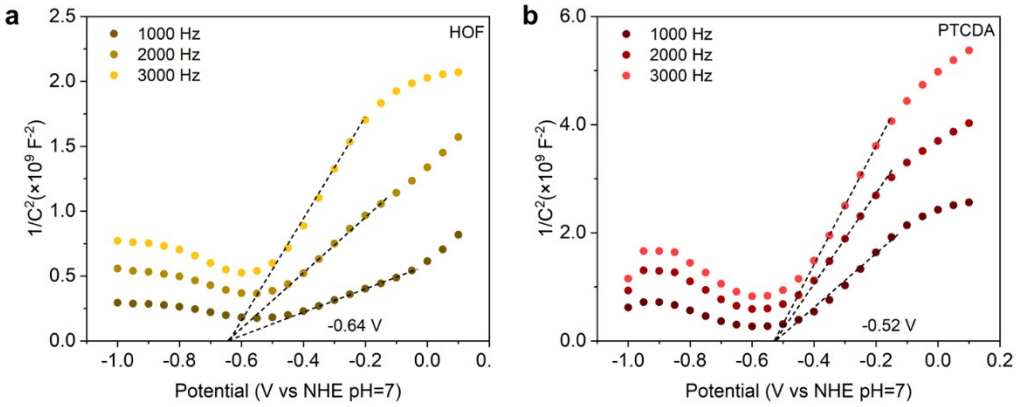

Fig. S5 Mott-Schottky plot of (a) HOF and (b) PTCDA.

The flat band potentials of HOF and PTCDA were determined to be -0.64 V and -0.52 V (vs. NHE, pH = 7), respectively, by extrapolating the linear region of the Mott-Schottky plots. Additionally, both HOF and PTCDA exhibit positive slopes in their Mott-Schottky plots, indicating n-type semiconductor characteristics.

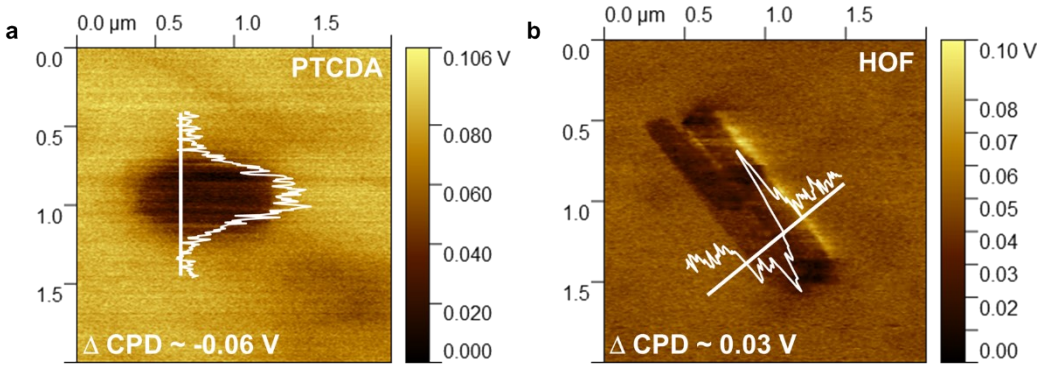

Fig. S6 Kelvin probe force microscopy (KPFM) test of PTCDA and HOF.

The work function and Fermi-level information of PTCDA and HOF were probed using Kelvin probe force microscopy (KPFM)[1]. The PTCDA and HOF suspension was coated on freshly dissociated HOPG and dried. The work function of HOPG was 4.65 eV. The work function of PTCDA and HOF can be calculated with equation (2):

$$\mathrm{WF\ (eV)} = 4.65 + e \times \mathrm{CPD} \qquad (2)$$

the CPD of PTCDA and HOF was probed as -0.06 and 0.03 V, respectively. Therefore, the work function of PTCDA and HOF can be calculated to be 4.59 and 4.68 eV, respectively.

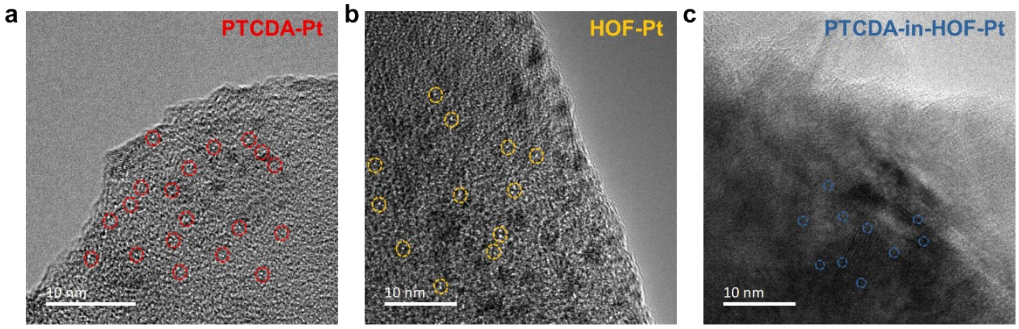

Fig. S7 HRTEM images of Pt deposited on (a) PTCDA, (b) HOF, and (c) PTCDA-in-HOF. (The part enclosed by the dotted line is Pt)

The Pt nanoparticles (indicated by the dotted circles) obtained via in situ photodeposition were observed on PTCDA, HOF, and PTCDA-in-HOF through HRTEM images (**Fig. S7**).

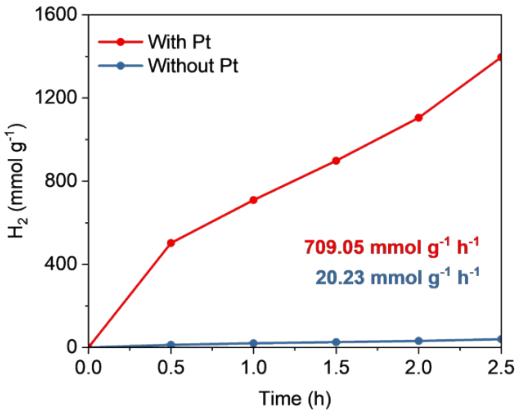

Fig.S8 The photocatalytic hydrogen evolution reaction (HER) performance of the PTCDA-in-HOF with and without Pt.

The intrinsic HER activity test of PTCDA-in-HOF (**Fig. S8**) shows that the hydrogen production rate reaches 20.23 mmol g^{-1} h^{-1} without Pt, which is 2.9% of the rate observed in the Pt-loaded system. This result confirms the critical role of Pt in enhancing charge separation and reducing the HER overpotential.

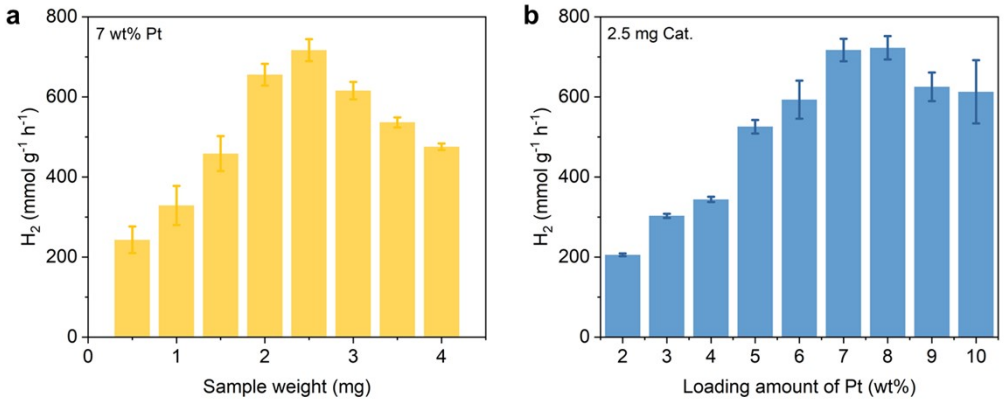

Fig. S9 Experimental conditions for photocatalytic hydrogen production (irradiated with a 300 W Xe light source, full-arc). (a) Comparison of photocatalytic H_2 evolution rates of PTCDA-in-HOF with different amounts of catalyst under full-arc irradiation ($\lambda \geq 350$ nm). (b) The comparison of photocatalytic H_2 evolution rate over PTCDA-in-HOF with different loading amounts of Pt under full-arc irradiation ($\lambda \geq 350$ nm). Data are presented as mean values ± standard deviation (n=3).

The PTCDA-in-HOF showed the best performance under the optimized conditions of 2.5 mg catalyst dosage and 7 wt% Pt co-catalyst deposition.

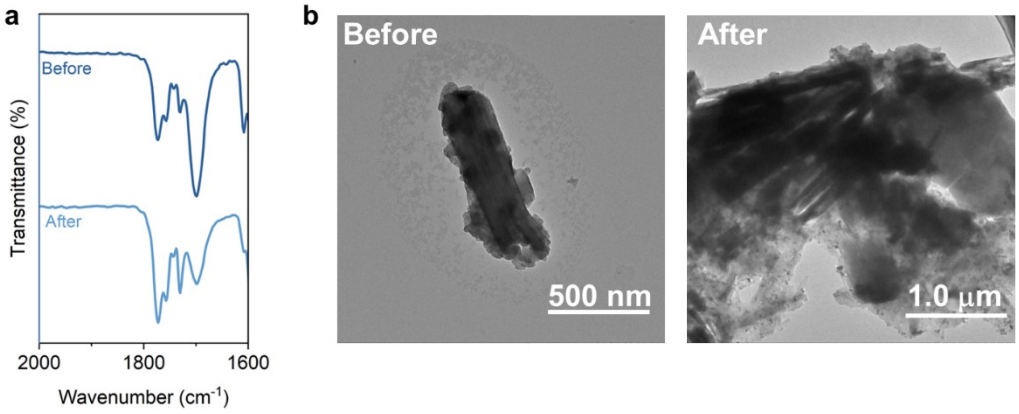

Fig. S10 (a) ATR FT-IR spectrum and (b)TEM images of PTCDA-in-HOF before and after reaction.

The ATR spectrum of the catalyst after the reaction shows no new characteristic vibrational or absorption bands, indicating no formation of new IR-active species (**Fig. S10a**). Changes in peak intensities likely result from surface active sites involved in adsorbing and activating the *H intermediate during hydrogen production. The reaction alters the local electron cloud density of functional groups, weakening the vibrational signals.

The TEM images (**Fig. S10b**) clearly demonstrate that PTCDA-in-HOF retains a uniform rod-like morphology both before and after the reaction, confirming its excellent structural stability.

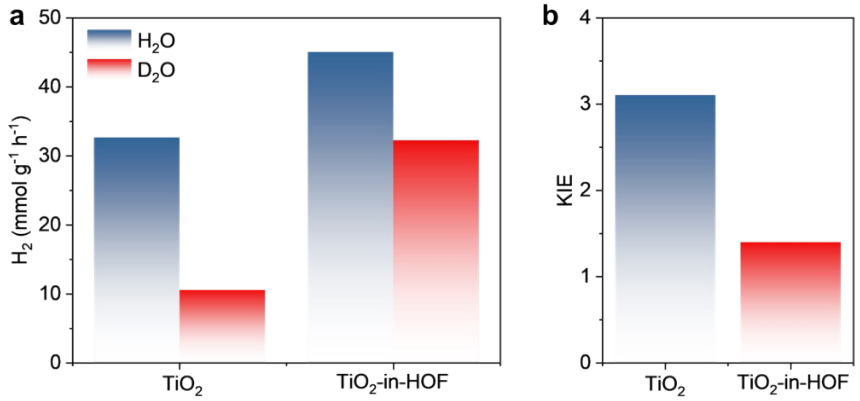

Fig. S11 (a) The photocatalytic hydrogen evolution performance of TiO_2 and TiO_2-in-HOF under the conditions of H_2O and D_2O. (b) Kinetic isotope effect (KIE) measurements for TiO_2 and TiO_2-in-HOF

The photocatalytic hydrogen evolution rates of TiO_2 and TiO_2-in-HOF were measured in H_2O and D_2O under identical reaction conditions. The HER rate for TiO_2 reached approximately 32.66 mmol·g^{-1}·h^{-1} in H_2O and about 10.52 mmol g^{-1} h^{-1} in D_2O. For TiO_2-in-HOF, the rates were approximately 45.07 mmol g^{-1} h^{-1} in H_2O and 32.26 mmol g^{-1} h^{-1} in D_2O (**Fig. S11a**).

The kinetic isotope effect (KIE) values, defined as the ratio of HER rates in H_2O versus D_2O, are presented. The KIE for TiO_2 (~3.1) indicates that proton transfer is the rate-determining step for pristine TiO_2. In contrast, the lower KIE observed for TiO_2 embedded in the HOF (~1.4) demonstrates that the HOF facilitates proton mobility, thereby reducing the kinetic limitation associated with proton transfer (**Fig. S11b**).

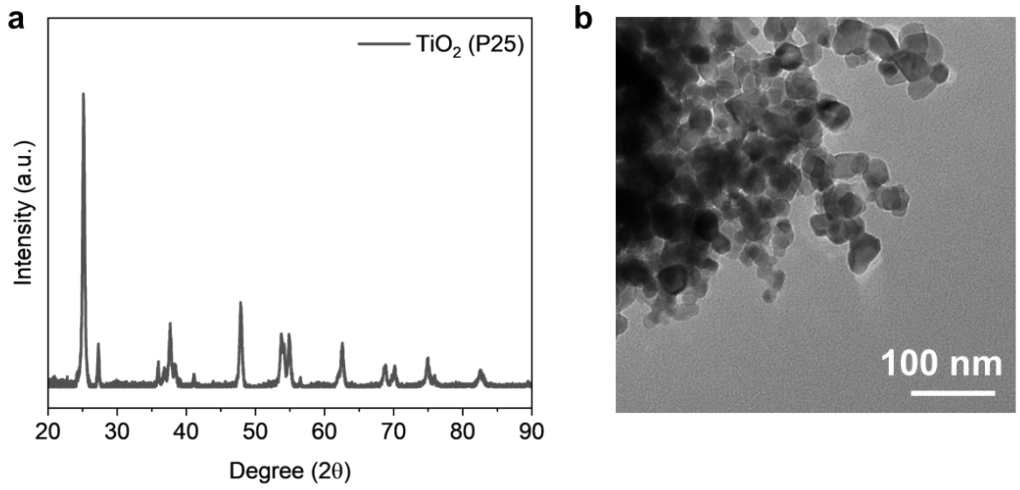

Fig. S12 (a) PXRD pattern and (b) TEM image of TiO_2 (P25).

The crystal structure and morphology of commercial TiO_2 (P25) were characterized. The PXRD spectrum (**Fig. S12a**) match the standard anatase-rutile mixed crystal phase of commercial P25, confirming its typical crystalline structure; the TEM image (**Fig. S12b**) shows the particles exhibit an irregular spheroidal/polyhedral morphology, with uniform size distribution, slight agglomeration, and sub-micrometer scale, consistent with the typical microscopic appearance with commercial P25.

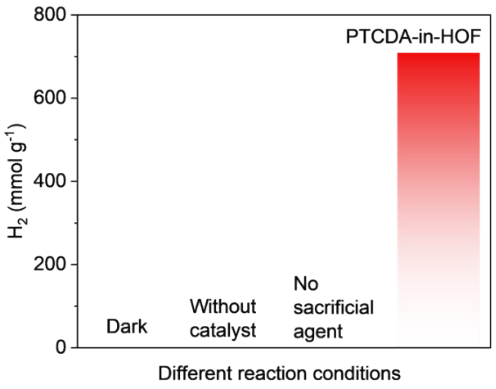

Fig.S13 The hydrogen production rate of PTCDA-in-HOF under different experimental conditions.

No H_2 was detected without light, catalyst, or sacrificial agent. Specifically, PTCDA-in-HOF produces H_2 only when exposed to light and in the presence of a sacrificial agent.

3. Additional Supplementary Tables

Table S1. Specific surface area and pore structure of as-prepared samples.

Sample	BET Surface Area ($m^2 \cdot g^{-1}$)	Langmuir Surface Area ($m^2 \cdot g^{-1}$)	Pore Volume ($cm^3 \cdot g^{-1}$)	Pore Size (nm)
HOF	303.71	329.63	0.33	1.26
PTCDA	13.46	14.21	0.06	4.72
PTCDA-in-HOF	146.07	157.18	0.23	1.32

Table S2. The TCSPC bi-exponential decay fitting data for HOF, PTCDA, and PTCDA-in-HOF.

Sample	B_1	B_2	τ_1	A_1	τ_2	A_2	τ_A
HOF	1.57	1193.07	5.56	0.01	1.36	0.99	1.38
PTCDA	5493.23	0.63	1.16	1.00	5.29	0	1.16
PTCDA-in-HOF	1.04	753427.79	5.25	0	0.73	1.00	0.73

The carrier lifetimes of HOF, PTCDA, and PTCDA-in-HOF were determined using time-correlated single-photon counting (TCSPC). The corresponding emission decay spectra were well fitted with a bi-exponential model (Equation 3-6), as shown below[4]:

$$I(t) = B_1 \times e^{-t/\tau_1} + B_2 \times e^{-t/\tau_2} \quad (3)$$

$$A_1 = \frac{B_1\tau_1}{B_1\tau_1 + B_2\tau_2} \quad (4)$$

$$A_2 = \frac{B_2\tau_2}{B_1\tau_1 + B_2\tau_2} \quad (5)$$

$$\tau A = \frac{B_1\tau_1^2 + B_2\tau_2^2}{B_1\tau_1 + B_2\tau_2} \quad (6)$$

where τ_1 and τ_2 (ns) denote the short and long fluorescence lifetimes, respectively; B_1 and B_2 are the weighting coefficients corresponding to τ_1 and τ_2. The average fluorescence lifetime, τ_A was further derived from the fitted parameters. Based on this analysis, the average lifetimes of HOF, PTCDA, and PTCDA-in-HOF were determined to be 1.38 ns, 1.16 ns, and 0.73 ns, respectively (**Table S2**).

Table S3. The summary of the photocatalytic performances of photocatalysts for hydrogen evolution from water splitting.

Catalysts	Co-catalyst	Sacrificial agent	Light Source	HER rate (mmol g^{-1} h^{-1})	AQE (%)	Ref.
PTCDA-in-HOF	7 wt% Pt	Ascorbic Acid	Full spectrum	**709.05**	29.4% (450 nm)	This work
HOF/COF	5 wt% Pt	Ascorbic acid	> 420 nm	390.68	61.35% (450 nm)	5
BBTT-1SO	3 wt% Pt	Ascorbic acid	380–780 nm	222.03	27.5% (500 nm)	6
PS/PSOS	3 wt% Pt	Ascorbic acid	380–780 nm	~ 60	26.2% (500 nm)	7
SA-DADK-H^+	4 wt% Pt	Triethanolamine	Full spectrum	278.2	25.1% (450 nm)	8
ZVCOFs	1 wt% Pt	Ascorbic acid	> 420 nm	~ 175	47.1% (420 nm)	9
COF-935	3 wt% Pt	Ascorbic acid	> 420 nm	67.55	3.39% (420 nm)	10
COF-954	5 wt% Pt	Ascorbic acid	AM 1.5G	< 60.53	4.09% (420 nm)	11
Co-DCdS	Co	Lactic acid	AM1.5G	60.1	56.7% (500 nm)	12
PITIC-ThF	3 wt% Pt	Ascorbic Acid	> 420 nm	55.8	4.76% (700 nm)	13
HOF-H_4TBAPy	5 wt% Pt	Ascorbic Acid	Full spectrum	357.93	28.35% (420 nm)	1
Bi-CBTP	1 wt% Pt	Ascorbic Acid	AM 1.5G	516.7	61.2% (420 nm)	14

Table S4. Wavelength-dependent AQE of photocatalytic H_2 evolution over PTCDA-in-HOF.

Wavelength (nm)	H_2 evolution in 1 hour (μmol)	Light intensity* (mW/cm^2)	Irradiation area (cm^2)	AQE (%)
380	84.96	99.19	1.00	14.98
400	153.48	102.49	1.00	24.88
420	192.57	121.59	1.00	25.06
450	196.30	98.54	1.00	29.42
500	204.14	99.43	1.00	27.29
550	180.73	109.36	1.00	19.97
590	77.84	90.21	1.00	9.72
650	14.43	65.28	1.00	2.26
700	2.43	59.16	1.00	0.39

*The light intensity is the actual light power of the incident light spot, which is measured by an optical power meter (Thorlabs, PM100D+S425C).

λ=450 nm：

The number of incident photons N:

$$N = \frac{E\lambda}{hc} = \frac{98.54 \times 1.00 \times 10^{-3} \times 1 \times 3600 \times 450 \times 10^{-9}}{6.626 \times 10^{-34} \times 3 \times 10^{8}} = 8.03 \times 10^{20} \quad (3)$$

AQE:

$$AQE = \frac{2 \times \text{the number of evolved } H_2 \text{ molecules}}{N} \times 100\%$$
$$= \frac{2 \times 6.02 \times 10^{23} \times 196.30 \times 10^{-6}}{8.03 \times 10^{20}} \times 100\% = 29.42\% \quad (4)$$

4. References

1. Q. Zhou, Y. Guo and Y. Zhu, *Nat. Catal.*, 2023, **6**, 574-584.
2. Y. Guo, W. Ma, M. Chong, C. Y. Tang, Q. Zhou, J. Nan and Y. Zhu, *Chem*, 2024, **10**, 1252-1267.
3. Z. Zhang, Y. Zhu, X. Chen, H. Zhang and J. Wang, *Adv. Mater.*, 2018, **31**.
4. C. Yang, Z. Zhang, P. Wang, P. Xu, T. Shen, M. Wang, Q. Zheng and G. Zhang, *J. Hazard. Mater.*, 2023, **451**.
5. R. Gao, R. Shen, C. Huang, K. Huang, G. Liang, P. Zhang and X. Li, *Angew. Chem. Int. Edit.*, 2024, **64**.
6. W. C. Lin, Y. H. Wu, Y. E. Sun, M. M. Elsenety, W. C. Lin, J. C. Yen, H. K. Hsu, B. H. Chen, H. Y. Huang, C. A. Chang, T. F. Huang, Y. R. Zhuang, Y. T. Tseng, K. H. Lin, S. D. Yang, C. H. Yu and H. H. Chou, *Angew. Chem. Int. Edit.*, 2024, **63**.
7. W.-C. Lin, Y.-E. Sun, Y.-R. Zhuang, T.-F. Huang, K.-J. Lin, M. M. Elsenety, J.-C. Yen, H.-K. Hsu, B.-H. Chen, C.-Y. Chang, J.-W. Chang, H.-N. Huang, B.-H. Li, S. Jungsuttiwong, T. Haldar, S.-H. Wang, W.-C. Lin, T.-L. Wu, C.-W. Chen, C.-H. Yu, A.-C. Su, K.-H. Lin, U. S. Jeng, S.-D. Yang and H.-H. Chou, *J. Am. Chem. Soc.*, 2024, **147**, 2537-2548.
8. X. Zhu, Y. Jia, Y. Liu, J. Xu, H. He, S. Wang, Y. Shao, Y. Zhai and Y. Zhu, *Angew. Chem. Int. Edit.*, 2024, **63**.
9. Z. Zhang and Y. Xu, *J. Am. Chem. Soc.*, 2023, **145**, 25222-25232.
10. K. Wang, Y. Zhong, W. Dong, Y. Xiao, S. Ren and L. Li, *Angew. Chem. Int. Edit.*, 2023, **62**.
11. Y. Zhong, W. Dong, S. Ren and L. Li, *Adv. Mater.*, 2023, **36**.
12. K. Yang, Y. Huang, T. Wang, Y. Li, Y. Du, J. Ling, Z. Fan, C. Zhang and C. Ma, *Adv. Mater.*, 2024, **36**.
13. M. H. Elsayed, M. Abdellah, A. Z. Alhakemy, I. M. A. Mekhemer, A. E. A. Aboubakr, B.-H. Chen, A. Sabbah, K.-H. Lin, W.-S. Chiu, S.-J. Lin, C.-Y. Chu, C.-H. Lu, S.-D. Yang, M. G. Mohamed, S.-W. Kuo, C.-H. Hung, L.-C. Chen, K.-H. Chen and H.-H. Chou, *Nat. Commun.*, 2024, **15**.
14. F. Yin, W. Wang, J. Zhang, S. Wan, B. Cheng, G. Luo, C. Wang, J. Yu and S. Cao, *Angew. Chem. Int. Edit.*, 2025, DOI: 10.1002/anie.202513602.